^{1}H-NMR Study of the Effect of Temperature through Reversible Unfolding on the Heme Pocket Molecular Structure and Magnetic Properties of *Aplysia limacina* Cyano-Metmyoglobin

Zhicheng Xia,* Bao D. Nguyen,* Maurizio Brunori,† Francesca Cutruzzolà,† and Gerd N. La Mar*
*University of California, Davis, Department of Chemistry, Davis, California; and †Dipartimento di Scienze Biochimiche "A. Rossi Fanelli", University of Rome "La Sapienza", Rome, Italy

ABSTRACT Two-dimensional ^{1}H NMR spectroscopy over a range of temperature through thermal unfolding has been applied to the low-spin, ferric cyanide complex of myoglobin from *Aplysia limacina* to search for intermediates in the unfolding and to characterize the effect of temperature on the magnetic properties and electronic structure of the heme iron. The observation of strictly linear behavior from 5 to 80 C° through the unfolding transition for all hyperfine-shifted resonances indicates the absence of significant populations of intermediate states to the cooperative unfolding with $T_m \sim 80°C$. The magnetic anisotropies and orientation of the magnetic axes for the complete range of temperatures were also determined for the complex. The anisotropies have very similar magnitudes, and exhibit the expected characteristic temperature dependence, previously observed in the isoelectronic sperm whale myoglobin complex. In contrast to sperm whale Mb, where the orientation of the magnetic axis was completely temperature-independent, the tilt of the major magnetic axis, which correlates with the Fe-CN tilt, decreases at high temperature in *Aplysia limacina* Mb, indicating a molecular structure that is conserved with temperature, although more plastic than that of sperm whale Mb. The pattern of contact shifts reflects a conserved Fe-His(F8) bond and π-spin delocalization into the heme, as expected for the orientation of the axial His imidazole.

INTRODUCTION

Myoglobins (Mb) are small (~150 residues) globular proteins usually consisting of eight (A–H) helices with a heme bound via the His F8 (eighth position on helix F), which function as carriers for molecular oxygen in muscle (1,2). The highly conserved fold, despite high sequence variability and relatively small size, has made Mb a paradigm for studying a variety of properties of proteins. One of these roles has been in the study of intermediates in a reversible denaturation of proteins, where mammalian apo-Mb at low pH undergoes a transition to a partially structured molten globule (3). The majority of folding studies have been on sperm whale apo-Mb. The Mb from the sea hare *Aplysia limacina* exhibits several novel properties relative to the typical mammalian Mbs. The characteristic H-bond to stabilize bound O_2 is provided by Arg E10 rather than the common His E7 (4), a position which, in *Aplysia* Mb, is occupied by Val. The heme pocket of *Aplysia* Mb also appears to be more loose or dynamically less stable, as witnessed by faster heme reorientation (5) and faster axial His labile proton exchange than in mammalian Mb (6) . Lastly, *Aplysia*, unlike the mammalian Mbs, readily denatures reversibly as the holo protein under the influence of a variety of perturbations such as temperature, pH, and chemical denaturation in the presence of urea (7,8). Optical studies on *Aplysia* apoMb have detected an intermediate in the thermal unfolding (9).

Our interests in this report are to assess the utility of ^{1}H NMR in characterizing the changes in structure brought about by elevation in temperature through the unfolding transition to obtain evidence for or against significant populations of intermediates before global unfolding. Because the hyperfine shifts, δ_{hf}s, of paramagnetic derivatives of Mbs are considerably more sensitive to perturbations remote from the heme cavity (10), we choose to study the low-spin, ferric metMbCN derivative whose ^{1}H NMR spectral parameters are the best understood of the paramagnetic Mb derivatives (10–14). The two components of δ_{hf}, are

$$\delta_{hf} = \delta_{dip} + \delta_{con}. \quad (1)$$

The dipolar (δ_{con}) and contact (δ_{con}) reflect dipolar and scalar influences of the paramagnetic iron on the ^{1}H chemical shifts. The more informative dipolar component is given by (10,15,16)

$$\delta^i_{dip} = (24\pi\mu_o N_A)^{-1}[3\Delta\chi_{ax}(3\cos^2\theta' - 1)R^{-3} + 2\Delta\chi_{rh}(\sin^2\theta'\cos 2\Omega')R]^{-3}\Gamma(\alpha,\beta,\gamma), \quad (2)$$

where R, θ', Ω' are the coordinates of proton i in an arbitrary, iron-centered coordinate, x', y', z', (based on the x-ray structure) as shown in Fig. 1, $\Delta\chi_{ax}$ and $\Delta\chi_{rh}$ are the axial and rhombic anisotropies of the paramagnetic susceptibility tensor, χ, in the magnetic coordinate system, x, y, z (shown in Fig. 1), and $\Gamma(\alpha, \beta, \gamma)$ represent the Euler angles, α, β, γ, that transform the reference into the magnetic coordinate

Submitted April 6, 2005, and accepted for publication July 27, 2005.

Address reprint requests to Maurizio Brunori, Tel.: 39-06-445-0291; E-mail: maurizio.brunori@uniroma1.it.

Zhicheng Xia's present address is Dept. of Chemistry, McGill University, Montreal, Quebec, Canada H3A 2K6.

Bao D. Nguyen's present address is Dept. of Chemistry, University of California, Irvine, CA 92697.

0006-3495/05/12/4149/10 $2.00

doi: 10.1529/biophysj.105.062398

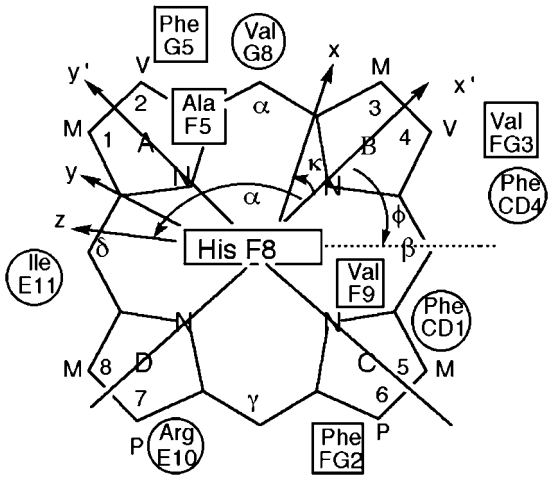

FIGURE 1 Structure of the heme with the reference coordinate system x', y', z' (R, θ', Ω') and magnetic coordinates system, x, y, z (R, θ, ϕ), shown. The x', y' plane is given by the mean plane of the heme in the crystal structure, with the x' axis passing through the pyrrole B nitrogen, and the z' axis normal to the heme and oriented to the proximal side. The positions relative to the heme of the residues whose proton dipolar shifts were used to generate the magnetic axes are also shown (proximal residues as *rectangles*, distal residues as *circles*). The angle α and $\kappa = \alpha + \gamma$ are defined; not shown is the angle β, which measures the tilt of the major magnetic axis, z, from the heme normal, z'.

system (16). The anisotropies reflect the strength of the axial bonds, and the sensitivity of the Euler angles reflects deformation of the symmetry from the pseudo-fourfold largely by the axial His imidazole plane orientation relative to the heme (17,18). The contact shift, related to the transferred unpaired π-spin density, ρ_i, is given by (15)

$$\delta^{i}_{con} = Q\rho_i Z/T, \tag{3}$$

where $Q \sim -63$ MHz for a pyrrole methyl, and Z is a constant for a given nucleus and electronic ground state. The pattern of δ^{i}_{con} for the four heme methyls reflects the orientation of the axial His imidazole relative to the heme (18–20) via the angle ϕ in Fig. 1. Even the slightest perturbation of the heme cavity environment due to perturbing of even a remote portion of the Mb has been shown to exert detectable changes in δ_{dip} and/or δ_{con} (10,11).

Previous detailed ^{1}H NMR studies on wild-type *Aplysia* metMbCN had provided comprehensive assignment (6,12) of the hyperfine-shifted heme cavity residues, and the search for a correlation between the observed and predicted δ_{dip} in Eq. 1 had also provided (12) the anisotropy and orientation of the paramagnetic susceptibility tensor at 30°C. Here we extend such studies on the *Aplysia* metMbCN over a temperature range up to 85°C. The two points of interest here will be whether the effect of temperature on the magnetic axes in *Aplysia* metMbCN confirm a looser heme pocket than in sperm whale metMbCN, and whether *Aplysia* metMbCN exhibits any evidence for significant population of an intermediate before its global unfolding at elevated temperature.

MATERIALS AND METHODS

Protein

Aplysia limacina Mb was isolated and purified as described in detail previously (21). The cyano-metmyoglobin complex, metMbCN, was prepared ~1 mM in ^2H_2O, 100 mM in phosphate, and 10 mM in KCN, at pH 8.3.

NMR spectroscopy

^{1}H NMR spectra was recorded on a Bruker AVANCE 500 spectrometer operating at 500 MHz (Bruker AXS, Madison, WI). Reference spectra from 5° to 85°C were collected over a 42.0 KHz bandwidth at a repetition rate of 2 s^{-1}.The spectra were exponentially apodized with 5-Hz line broadening. NOESY spectra (22) (60-ms mixing time) in 10° intervals between 5° and 85°C were recorded at 500 MHz over a 30 kHz bandwidth using 256 t1 blocks of 64 scans each and 2048 t2 points at a repetition rate of 3 s^{-1}. The two-dimensional data sets were apodized by 30°-shifted-sine bell-squared function and zero-filled to 2048 × 2048 points before Fourier transformation.

Optical and CD spectra

Thermal denaturation was carried out by equilibrating a 5- or 10-μM protein solution in 0.1 M sodium phosphate buffer, pH 8.1, containing 2 mM sodium cyanide, between 20 and 92°C. The reversibility was found to be >90%. The optical spectra were recorded on a Hewlett-Packard 8453 spectrophotometer (Palo Alto, CA) and the circular dichroic spectra on a Jasco J715 spectrometer (Tokyo, Japan), both equipped with a Peltier cell. Circular dichroic spectra were measured between 200 and 300 nm both at single temperature values and by increasing the temperature by 1°C/min between 20 and 92°C. The data were analyzed according to a standard two-state equation (23) for thermal unfolding,

$$\Delta G_{D-N(T2)} = \Delta H_{D-N(T1)} + \Delta C_p(T_2 - T_1) - T_2(\Delta S_{D-N(T1)} + \Delta C_p(T_2/T_1)), \tag{4}$$

where ΔC_p was estimated from the size of the protein and from literature data (24,25). Variation of the value of ΔC_p does not affect the calculation of the free energy of unfolding. Three measurements were averaged to determine the T_m.

Magnetic axes determination

The anisotropies, ($\Delta\chi_{ax}$, $\Delta\chi_{rh}$), and orientation (α,β), of the paramagnetic susceptibility tensor, χ, were determined from a five-parameter, least-squares search for the minimum in the error function, F/n (10,16,26):

$$F/n = \sum_{i=1}^{n} |\delta_{dip}(obs) - \delta_{dip}(calc)|^2. \tag{5}$$

Error analyses were performed with the Levenberg-Marguard method with boundaries of the error function, F/n, set equal to 95.4% of the confidence limit (27,28). The δ_{dip}(calc) are given by Eq. 2, and the observed dipolar shifts for noncoordinated residues are given by

$$\delta_{dip}(obs) = \delta_{DSS}(obs) - \delta_{DSS}(dia), \tag{6}$$

where δ_{DSS}(obs) is the observed chemical shift, referenced to DSS, for metMbCN, and δ_{DSS}(dia) is the chemical shift, referenced to DSS, for a diamagnetic structural analog. In the absence of NMR data for a diamagnetic analog, such as MbCO, δ_{DSS}(dia) have been reliably estimated (29,30) by available programs for determining chemical shifts in folded proteins (31,32), to which are added the ring currents of the heme

(33). The *Aplysia* metMbCN crystal structure (34) was used. The contact shift, δ_{con}, for ligands to the iron (heme and axial His) were determined via

$$\delta_{con} = \delta_{DSS}(obs) - \delta_{DSS}(dia) - \delta_{dip}(calc). \quad (7)$$

RESULTS

Optical studies

The thermal unfolding profile of *Aplysia* metMbCN was monitored by far UV-CD and absorbance spectroscopy. As shown in Fig. 2, a single cooperative transition is seen by CD with a $T_m = 354.1 \pm 1$ K (81°C); the same behavior is seen following the transition at 423 nm (data not shown). The position of the high-temperature absorbance supports the removal of the heme from the specific environment provided by the hydrophobic pocket, but does not shed light on whether the only His present in the protein, His F8, is still bound to the heme iron.

^{1}H NMR studies

The 500 MHz ^{1}H NMR spectra of *Aplysia* metMbCN as a function of temperature in the range 15–86°C are illustrated in Fig. 3. The resonances in the resolved portion of the spectral window (outside the 0–10 ppm diamagnetic portion), as well as the majority of nonresolved but hyperfine-shifted residue protons, have been unambiguously assigned and reported previously (6,12), and the peaks are labeled accordingly in Fig. 3. We address only the major (~75%) heme orientational isomer in solution; resolved peaks for the minor component (previously assigned (6)) are marked by small stars.

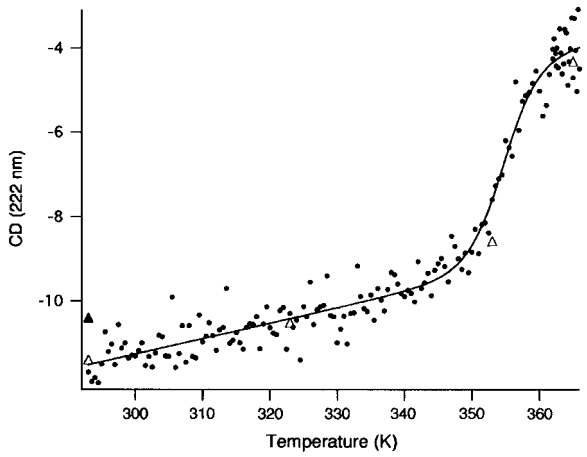

FIGURE 2 Thermal denaturation of *Aplysia* metMbCN as a function of temperature in the range 20–92°C (293–365 K) in 100 mM phosphate pH 8.1 and 2 mM NaCN. The graph shows the CD data at 222 nm recorded at 1° intervals on a 4-μM protein solution (light path = 0.1 cm). The open triangles on the main graph are points recorded at single temperature values after equilibrating the protein solution for 10 min. The solid triangle indicates the value corresponding to a protein solution kept at 92°C for 10 min and slowly cooled down to 20°C. The continuous line is a fit to Eq. 4.

It is observed that all resolved resonances change chemical shifts with increasing temperature, with the shifts of the majority of the signals approaching the diamagnetic spectral window, as expected for the approximate Curie law for the spin magnetization (10,15,19,20,35). However, at ~75°C, prominent, narrow, new composite signals appear in the 0–10 ppm window whose intensities increase dramatically at higher temperature (Fig. 3, *D–F*). The intensities of the hyperfine-shifted resonances decrease until 80°C, where all chemical-shift dispersion indicative of a folded protein is lost, with the most dramatic change obvious in the aromatic spectral window 5–10 ppm. The loss of spectral dispersion in the diamagnetic spectral window 0–10 ppm, and the loss of the hyperfine-shifted signal, are taken as direct evidence that the protein has unfolded. It was not possible to detect at 85°C any hyperfine-shifted and relaxed signals in the −30 to 10 and 0–45 ppm window that would arise from a paramagnetic hemin (36,37). The ^{1}H NMR spectra are completely reversible with temperature. Although some precipitation occurred near 75°C in several instances, the protein redissolved, and the ^{1}H NMR spectra were completely reproducible, upon cooling. The NMR data are also consistent with cooperative unfolding with a T_m ~77°C. The value is consistent with that obtained by UV-CD and visible spectroscopy, considering that the protein concentration and the pH are different in the two studies.

The chemical shifts for previously assigned protons experiencing significant dipolar shifts (6,12,30), which can be expected to occupy relatively fixed positions in the complex (i.e., no flexible long-chain termini), and which were assignable over the complete temperature range, were determined in ~10° intervals over the temperature range 7–85° (not shown). The plots of chemical shift versus reciprocal absolute temperature (Curie plot) for the heme methyls and meso-Hs, and the axial His(F8) $C_\beta H$ are shown in Fig. 4. Similar representative data for the Phe_{98}(FG2) variant's hyperfine-shifted proton's signals for the nonligated residues (see Supplementary Material for data on other residues) are illustrated in Fig. 5. The variable temperature data for the iron ligands, the porphyrin methyls, meso-Hs, and axial His(F8) $C_\alpha H$, all fall on a straight line over the whole temperature range, including the unfolding, and give no hint of deviations indicative of population of intermediates even at the highest temperature. The nonligated residues that exhibit significant dipolar shifts (12,30) such as Phe_{98}(FG2) (Fig. 5), Phe_{91}(F4), Phe_{43}(CD1), and Val_{63}(E7) (not shown; see Supplementary Material), among others, exhibit similarly straight lines through the unfolding transition.

Magnetic axes

The magnetic axes determination used the observed dipolar shifts for all protons or residues that can be expected to occupy unique and fixed positions relative to the iron, as defined by the coordinates of an *Aplysia* Mb crystal structure

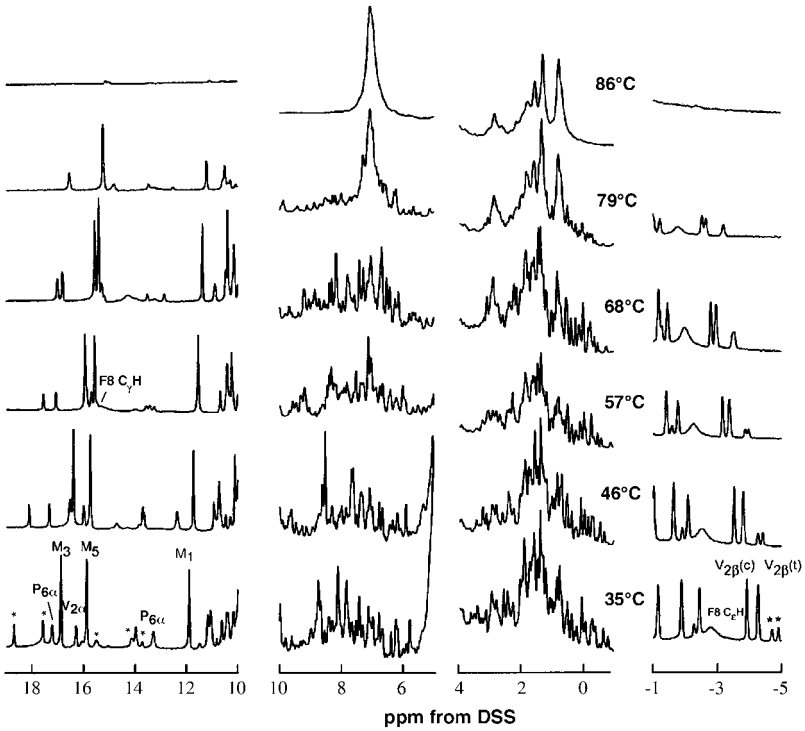

FIGURE 3 500 MHz ^{1}H-NMR spectra of *Aplysia* metMbCN as a function of temperature at pH 8.6. The previously assigned (12,30) resolved peaks are labeled for the major isomer (~75%) in solution (M = methyl, P = propionate, and V = vinyl); minor component (~25%) peaks are marked by small stars.

(34,38) and are readily assignable in the relative brief times (~30 min) allowed for NOESY spectrum collection at elevated temperatures. These residues are identified in the caption to Fig. 6. The δ_{dip}(obs) values, as a function of temperature (not shown), were used to carry out five-parameter searches for the anisotropies, $\Delta\chi_{ax}$ and $\Delta\chi_{rh}$, and the three Euler angles, α, β, and γ, for which β defines the tilt of the major (i.e., z-) magnetic axis from the heme normal, α represents the direction of the tilt, and γ is defined by the angle between the projection of the major magnetic axis on the heme plane and the x' axis. The location of the x,y, or rhombic, axes is approximated by $\kappa \sim \alpha + \gamma$; the three angles α, β, and κ are

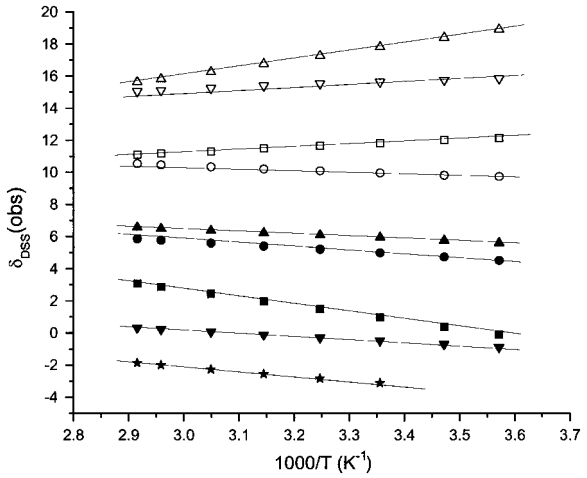

FIGURE 4 Plot of δ_{DSS}(obs) versus reciprocal absolute temperature (Curie plot) for the iron-ligated heme and axial His(F8) protons of *Aplysia* metmbCN in ^2H_2O, 100 mM in phosphate, pH 8.6; 1-CH_3 (□), 3-CH_3 (△), 5-CH_3 (▽), 8-CH_3 (○), α-meso-H (■), β-meso-H (▲), γ-meso-H (▼), δ-meso-H (●), and His(F8) C_αH (★).

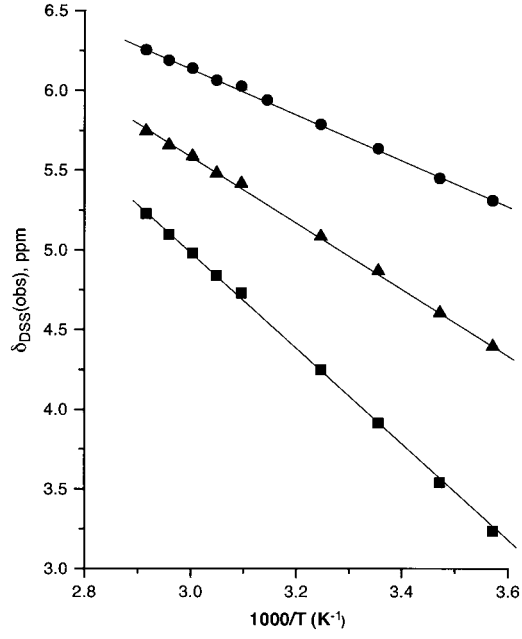

FIGURE 5 Plot of δ_{DSS}(obs) versus reciprocal absolute temperature (Curie plot) of nonligated $Phe_{\sigma 8}$(FG2) in *Aplysia* metMbCN in ^2H_2O; the solid circles, squares, and triangles represent C_δHs, C_εHs, and C_ζH shifts, respectively.

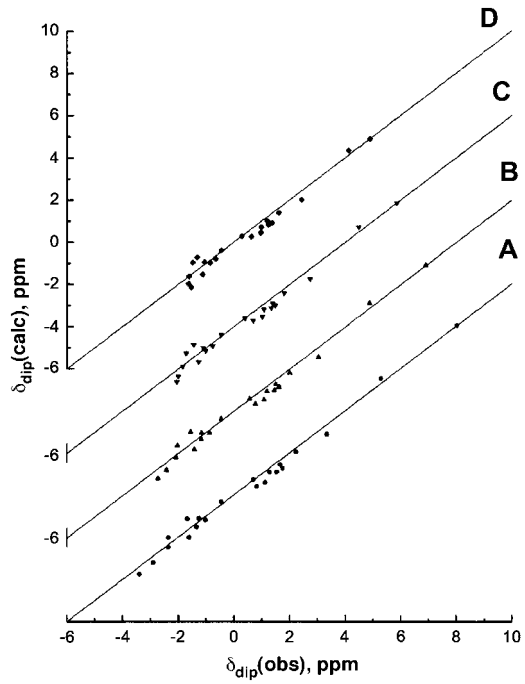

FIGURE 6 Plot of δ_{dip}(obs), obtained via Eq. 6 versus δ_{dip}(calc) obtained from the optimized magnetic axes (Eqs. 2 and 5) as a function of temperature, with the parameter for each temperature listed in Table 1, at (*A*) 7°C, (*B*) 25°C, (*C*) 47°C, and (*D*) 68°C. The 21 inputs include: F_{43}(CD1) $C_\alpha H$; F_{46}(CD4) $C_\alpha H$, $C_\delta Hs$, $C_\varepsilon Hs$; I_{67}(E11) $C_\alpha H$; A_{92}(F5) $C_\alpha H$, $C_\beta H_3$; H_{95}(F8) $C_\alpha H$; V_{96}(F9) $C_\beta H$, $C_{\gamma 1}H_3$, $C_{\gamma 2}H_3$; F_{98}(FG2) $C_\delta Hs$, $C_\varepsilon Hs$, $C_\zeta H$; V_{100}(FG4) $C_{\gamma 1}H_3$, $C_{\gamma 2}H_3$; F_{105}(G5) $C_\zeta H$; and V_{108}(G8) $C_\alpha H$, $C_\beta H$, $C_{\gamma 1}H$, $C_{\gamma 2}H$.

depicted in Fig. 1. For each temperature, very low minima in the residual error function, F/n (Table 1), in the least-squares searches, were found at all temperatures between 7° and 68°C, and the correlation between δ_{dip}(obs) and δ_{dip}(calc) at each temperature is quite good, as illustrated in Fig. 6. The five determined parameters are listed in Table 1 as data sets II–VIII.

The magnetic axes and anisotropies were also determined at 25°C using the more extensive assignments previously reported (12,30) (Table 1, data set *I*). The 25°C orientation, $\alpha = 97 \pm 8°$, $\beta = 11.6 \pm 0.5$, and $\kappa = 27 \pm 5°$, and anisotropies, $\Delta\chi_{ax} = 2.22 \pm 0.06 \times 10^{-8}$ m^3/mol and $\Delta\chi_{rh} = -0.55 \pm 0.06 \times 10^{-8}$ m^3/mol, are consistent with the earlier determination (30) where the latter parameters are adjusted for the redefinition (29) of the reference frame through pyrrole Ns, rather than meso-carbons (30), and the reference of α to the positive, rather than negative x-axis. The results of the magnetic axes determination at 25°C (Table 2, data set *II*) using the 21 input data sets available through the temperature range 7–68°C, are observed to be within the uncertainties of the parameters using the larger data set.

Both anisotropies exhibit straight lines in a plot of $\Delta\chi_{ax}$ and $\Delta\chi_{rh}$ versus reciprocal absolute temperature (Curie plot), as illustrated in Fig. 7 *B*. The systematic, and expected (17,39), temperature dependence of the anisotropies, is further support for the accuracy of the magnetic axes determination. The values of the angles, α, β, and κ, as a function of temperature, are similarly graphed in Fig. 7 *A*. The direction of the tilt, α, and the rhombic axes, κ, are essentially independent of temperature. The magnitude of the tilt, β, however, decreases slightly, but systematically, with increasing temperature, as shown in Fig. 8 *A*. Although the determination of magnetic axes using different *Aplysia* Mb crystal coordinates (34,38) resulted in small differences in the five parameters (30) (in large part due to the different definition of the reference coordinate system due to variable nonplanarity of the heme), the effect of temperature on the parameters was essentially independent of the crystal coordinates (not shown).

Factoring the heme and His(F8) hyperfine shifts

The quantitative determination of the magnetic axes in the temperature range 5–68°C provides the δ_{dip}(calc) that allows determination of δ_{con} via Eqs. 2 and 7. The resulting δ_{con} at 25°C for the four heme methyls, four meso protons, and the axial His_{96}(F8), are listed in Table 2, where they can be compared to similar data previously reported for sperm whale metMbCN (29). With the well-behaved magnetic axes anisotropies with variable temperature (Fig. 7 *A*), it is possible to generate δ_{dip}(calc), and hence δ_{con}, over the complete temperature range 5–68°C. The Curie plots for the heme methyl δ_{con} are illustrated in Fig. 8.

DISCUSSION

Unfolding of *Aplysia* metMbCN

The change in far UV CD spectrum as a function of temperature (shown in Fig. 2) is characteristic of the cooperative unfolding with a melting temperature of ~81°C. Although the features of the CD spectrum at the end of the transition (92°C) do not allow a reliable calculation of the residual secondary structure content, the comparison of this spectrum with that of a fully unfolded *Aplysia* metMbCN in 7 M urea (not shown) at 25°C indicates that some CD signal is still present at 92°C. This finding is not incompatible with a residual secondary structure content in the high-temperature denatured state. The intrinsic stability of *Aplysia* myoglobin to temperature denaturation is reflected in the behavior of the apoprotein (9) and is unchanged in a site-directed mutant, where the Trp_{130} in the H helix was replaced by a Tyr (40). The ^{1}H NMR data in Fig. 3 show that the well-dispersed ^{1}H NMR spectrum in both the diamagnetic (0–10 ppm) and hyperfine-shifted (17–10 and 0–7 ppm) windows loses intensity above 55° and is replaced by a spectrum solely within the 1–7 ppm diamagnetic window, with dispersion characteristic of the amino acid composition of the protein. This loss of dispersion is most apparent in the aromatic window

TABLE 1 Magnetic axes determinations for *Aplysia* metMbCN

Data Set†	N‡	T, °C	α§	Orientation* β§	Orientation* $\kappa = \alpha + \gamma$§	$\Delta\chi_{ax} \times 10^{-8}m^3/mol$¶	$\Delta\chi_{rh} \times 10^{-8}m^3/mol$¶	F/n,* (ppm)^2
I¶	77	25	97 ± 4	11.7 ± 0.5°	27 ± 5	2.22 ± 0.06	−0.55 ± 0.06	0.05
II‖	21	7	106 ± 5	12.5 ± 0.5°	26 ± 4	2.63 ± 0.08	−0.79 ± 0.09	0.06
II	21	15	106 ± 5	12.3 ± 0.6°	26 ± 4	2.48 ± 0.08	−0.72 ± 0.09	0.06
II	21	25	105 ± 5	11.8 ± 0.6°	26 ± 4	2.34 ± 0.08	−0.62 ± 0.09	0.06
II	21	35	105 ± 6	11.5 ± 0.7°	24 ± 5	2.20 ± 0.08	−0.55 ± 0.09	0.06
II	21	46	105 ± 7	11.1 ± 0.7°	24 ± 7	2.06 ± 0.09	−0.49 ± 0.09	0.07
II	21	57	105 ± 8	10.0 ± 0.8°	24 ± 8	1.92 ± 0.9	−0.43 ± 0.09	0.07
II	21	68	105 ± 9	10.2 ± 0.8°	24 ± 9	1.82 ± 0.09	−0.38 ± 0.10	0.07
III**		25	150 ± 10	15.8 ± 0.6°	−10 ± 5	2.48 ± 0.10	−0.59 ± 0.10	

*Residual error function, (Eq. 4), after minimization.
†Input δ_{dip}(obs) data set.
‡Number of protons in each input data set.
§Euler angles, in degrees, as defined for Eq. 2 and in Fig. 1.
¶Data set *I* used all residues with a proton with $\delta_{dip} > |0.5|$ppm, and was presented previously (30).
‖Data set *II* consists of expected rigid protons with significant δ_{dip}(obs) which are unambiguously assigned at all temperatures; they are identified in the caption to Fig. 6.
**Magnetic axes and anisotropies reported for sperm whale metMbCN (29).

5–8 ppm in Fig. 3 *E*. Although the optical and ^{1}H NMR data agree on the loss of most of the tertiary and secondary structures, it is not clear whether the Fe-His(F8) bond is retained above 75°C. Free hemin should lead to resolved methyl peaks in the 10–18 ppm spectral window in the presence of the excess cyanide, which are not seen (36,37). Alternatively, a His-Fe^{+3}-CN$^-$ linkage should similarly exhibit resolved peaks for both heme and His C_βHs. The failure to observe any hyperfine-shifted signals outside the 1–7 ppm window at the elevated temperatures does not provide a definitive answer. The likely case is that the hydrophobic hemin, as a His-Fe^{+3}-CN$^-$ or NC-Fe^{+3}-CN$^-$ species, is still associated within limited, loosely structured portions of the unfolded protein, and the heterogeneity of numerous such environments leads to severe line broadening that renders the hyperfine-shifted peaks undetectable.

The heme hyperfine shifts are extraordinarily sensitive probes of the orientation of the axial His relative to the heme

TABLE 2 Factoring hyperfine shifts for heme and His(F8) of *Aplysia* metMbCN

Proton	*Aplysia* metMbCN δ_{DSS}(obs)*	δ_{DSS}(dia)†	δ_{hf}‡	δ_{dip}(calc)§	δ_{con}¶	Sperm whale MetMbCN δ_{con}‖
Heme						
1-CH_3	11.80	3.6 ± 0.1	8.2 ± 0.1	−2.8 ± 0.3	11.0 ± 0.4	18.0 ± 0.2
3-CH_3	17.79	3.6 ± 0.1	14.2 ± 0.1	−5.0 ± 0.4	19.2 ± 0.5	6.0 ± 0.2
5-CH_3	15.62	2.8 ± 0.2	12.8 ± 0.1	−3.3 ± 0.3	15.3 ± 0.4	27.5 ± 0.2
8-CH_3	9.95	3.6 ± 0.1	6.3 ± 0.1	−4.0 ± 0.3	10.4 ± 0.4	14.7 ± 0.2
6-H_αs**	16.5	3.5 ± 0.5	13.0 ± 0.5	−3.6 ± 0.8	16.6 ± 1.3	
7-H_αs**	4.3	3.5 ± 0.5	0.8 ± 0.5	−4.5 ± 1.0	5.3 ± 1.5	
α-meso-H	0.96	10.0 ± 0.5	−9.0 ± 0.5	−11.7 ± 1.2	2.7 ± 1.7	6.6 ± 0.5
β-meso-H	5.93	10.0 ± 0.5	−4.1 ± 0.5	−8.3 ± 1.0	4.2 ± 1.5	2.8 ± 0.4
γ-meso-H	−0.44	10.0 ± 0.5	−10.4 ± 0.5	−12.9 ± 1.4	2.5 ± 1.9	6.3 ± 0.4
δ-meso-H	4.99	10.0 ± 0.05	5.0 ± 0.5	−6.9 ± 1.1	1.9 ± 16	6.1 ± 0.5
His(F8)						
$C_{\beta 1}$H	10.55	1.2 ± 0.2	9.3 ± 0.2	6.5 ± 0.8	2.8 ± 1.0	3.4 ± 0.2
$C_{\beta 2}$H	10.73	1.2 ± 0.2	9.5 ± 0.2	6.8 ± 0.8	2.7 ± 1.0	0.8 ± 0.2
C_εH	−2.35	1.6 ± 0.2	−4.0 ± 0.2	18.0 ± 2.0	−22.0 ± 2.0	19.0 ± 1
C_δH	18.35	1.3 ± 0.2	−17.0 ± 0.2	25.0 ± 3.0	−8.0 ± 3.0	−1.1 ± 0.8
N_δH	14.30	9.0 ± 1.0	5.3 ± 1.0	9.9 ± 0.9	−4.6 ± 1.9	−3.5 ± 0.3

*Chemical shift in ppm, referenced to DSS, in ^2H_2O at pH 8.6 and 25°C.
†Chemical shift of a diamagnetic structural analog.
‡Hyperfine shift, in ppm at 25°C, defined as δ_{DSS}(obs)−δ_{DSS}(dia).
§Dipolar shift, in ppm at 25°C, as calculated from the optimized magnetic axes for data set *II* in Table 1.
¶Contact shift, in ppm at 25°C, obtained from Eqs. 1 and 2.
‖Previously reported (29) contact shift, in ppm at 25°C, for sperm whale metMbCN in ^2H_2O at pH 8.6.
**Mean of the geminal protons.

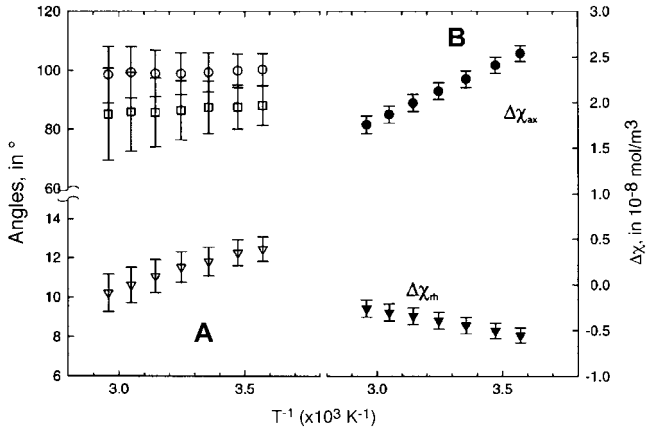

FIGURE 7 Plot of (*A*) angles, α, β, and κ, that define the orientation of the magnetic axes; and (*B*) the magnetic anisotropies determined from five-parameter least-square searches over the temperature range 7–68°C. The uncertainties in each parameter are given by vertical error bars.

(10,18–20,41), whereas the axial His(F8) hyperfine shifts are extremely sensitive to both the nature of the Fe-His(F8) bond and the heme Fe-CN tilt (10,17,29,39). The solely dipolar shifts for the nonligated residues are exquisitely sensitive probes for the disposition of the residue relative to the heme, the magnetic axes, and anisotropies. The surprisingly well-behaved Curie plots for heme (Fig. 4), His(F8) (Fig. 4), and nonligated residue (Fig. 5) protons over the complete temperature range 5–79°C provide compelling evidence against detectable populations of any partially unfolded intermediate, which influences the heme environment.

The unfolding temperature of *Aplysia* metMbCN is higher than that reported for other derivatives of the same protein (7), which is, to a first approximation, consistent with a greater value of the folding free energy for cyanomet derivatives. The superior solubility properties and ^{1}H NMR spectral parameters highly sensitive to even minor structural perturbations are expected to significantly improve the prospects for detecting partially unfolded intermediates for *Aplysia* metMbCN mutants.

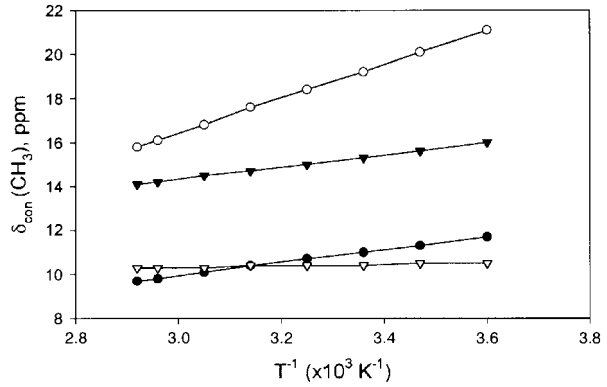

FIGURE 8 Plot of δ_{con} versus reciprocal absolute temperature (Curie plot) for the heme methyls (1-CH_3, ●; 3-CH_3, ○; 5-CH_3, ▼; and 8-CH_3, ▽).

Magnetic properties

The similarly detailed orientation and anisotropies, as well as their temperature dependence, for sperm whale metMbCN have been reported previously (29). The axial anisotropies are consistently ~5% smaller for *Aplysia* ($2.34 \pm 0.08 \times 10^{-8}$ m^3/mol at 25°C) than sperm whale ($2.48 \pm 0.08 \times 10^{-8}$ m^3/mol at 25°C). The rhombic anisotropies are essentially the same at $-0.60 \pm 0.10 \times 10^{-8}$ m^3/mol. Moreover, the temperature dependence for both $\Delta\chi_{ax}$ and $\Delta\chi_{rh}$ for *Aplysia* metMbCN is essentially the same as reported for sperm whale metMbCN (29), both of which are consistent with the theoretical predictions of Horrocks and Greenberg (17,39).

The magnitude and direction of the tilt of the major magnetic axes in *Aplysia* metMb were shown to be consistent with an interaction of the Arg_{60}(E10) $N_\varepsilon H$ with the bound cyanide in both solution (30) and crystal (34). The different orientation and larger tilt of the major magnetic axis, and hence Fe-CN vector, in sperm whale metMbCN to provide a stabilizing H-bond to the ligated cyanide, have been rationalized by steric interaction with Val_{68}(E11) (16,42). The rhombic axes are predicted to follow the counter-rotation rule, where κ is related to the angle, ϕ (but in opposite direction), of the axial His(F8) imidazole plane relative to the x' axis (18–20,41) (Fig. 1). The $\kappa \sim -10 \pm 10°$ in sperm whale Mb is consistent (29,43) with the $\phi \sim 0°$. The much larger $\kappa \sim 27 \pm 10°$ for *Aplysia* metMbCN is similarly consistent (34,38) with $\phi \sim 35°$.

The asymmetry in hyperfine shifts for the heme pyrrole substituents is dominated by contact shifts (10,18–20) (see below), whereas those for the meso-Hs have been shown (10,11,44,–48) to be dominated by the dipolar shifts. Thus, the observed 25°C chemical shift parameter (44,46–48) is

$$\begin{aligned}\Delta\delta\text{-(mesoH)} &= \delta_{DSS}(\alpha\text{-meso-H}) - \delta_{DSS}(\beta\text{-meso-H}) \\ &\quad + \delta_{DSS}(\gamma\text{-meso-H}) - \delta_{DSS}(\delta\text{-meso-H}) \\ &= -10.4\,\text{ppm} \qquad (8)\end{aligned}$$

(see Table 2), which is indistinguishable from the predicted value at 25°C $\Delta(\delta_{dip}) = \delta_{dip}(\alpha\text{-meso-H}) - \delta_{dip}(\beta\text{-meso-H}) + \delta_{dip}(\gamma\text{-meso-H}) - \delta_{dip}(\delta\text{-meso-H}) = -9.4 \pm 2.3$ ppm (see Table 2).

Electronic structure

The factored hyperfine shifts for the heme and axial His(F8) are given in Table 2. The pattern of δ_{con} for the axial His are very similar to those reported previously (29) for sperm whale metMbCN. The apparent slightly larger δ_{con} for the axial His(F8) (Table 2) and the slightly smaller $\Delta\chi_{ax}$ (Fig. 6) in *Aplysia* than sperm whale metMbCN suggest that the His(F8)-Fe bond might be slightly stronger in the former than the latter metMbCN complex. The orientation of a His(F8) with the imidazole plane close to parallel to N-Fe-N

vector ($\phi \sim 0°$ in Fig. 1) has been associated (49) with the introduction of some strain in the axial bond in a six-coordinate complex due to steric interaction between the axial His $C_\varepsilon H$ and $C_\delta H$ with the two *trans* pyrrole nitrogens of the heme. This steric effect, for *Aplysia* Mb, must be small, since the His ring is oriented (34,38) with ϕ near 35° (Fig. 1). The stronger His(F8)-Fe bond would increase the $(d_{xz}, d_{yz})-d_{xy}$ spacing that leads to a reduction of $\Delta\chi_{ax}$, and an increase (17) in His(F8) δ_{con}. Unfortunately, although these trends are observed, the parameters are not clearly distinguishable outside the uncertainties. Studies in progress on the cyanomet complex of leghemoglobin, for which stronger His(F8)-Fe bonding due to $\phi \sim 40°$ has been proposed (49), may shed further light on this potential correlation among $\Delta\chi_{ax}$, δ_{con}(His(F8)), and ϕ.

The pattern of δ_{con} for the heme methyls in *Aplysia* metMbCN (6), on the other hand, differs significantly from that in sperm whale metMbCN (50,51). The value of Q in Eq. 3 is given by $Q = A\cos^2\Psi$, where Ψ is the H-C-C_π-z^* dihedral angle (10,15) (z^* is the normal to the heme through C_π). For a methyl group, $\langle\cos^2\Psi\rangle = 0.50$, while for the most common methylene orientation, where $\Psi = 60 \pm 10°$ for each proton, $\cos^2\Psi = 0.25$. Hence the same ρ_π in Eq. 3 will lead to δ_{con} only half as large for a propionate $C_\alpha H$ as for a methyl. Thus, the largest π-spin density (via Eq. 3) appears for the positions 1-, 2-, and 6-positions. This pattern is qualitatively consistent with the symmetry properties of the two $3e_\pi$ molecular orbitals (10,37), determined by the orientation of the axial His imidazole plane relative to the heme.

The determination of the orientation and anisotropies of the paramagnetic susceptibility tensor over the temperature range 7–68°C provides quantitative data for δ_{dip} for the heme methyls at each temperature, and hence, provides δ_{con} as a function of temperature. A plot of δ_{con}(heme CH_3) versus T^{-1} is shown in Fig. 7. It is observed, typical for low-spin ferric hemoproteins (10,20,35), that the temperature dependence of δ_{con} for the four methyls differ, in that two exhibit stronger temperature dependence than Curie (T^{-1}) and two exhibit weaker temperature dependence than T^{-1} (but do not exhibit anti-Curie, i.e., negative slope). This behavior is indicative of thermal populations of the excited component of the $3e_\pi$ MO, as discussed in detail for other low-spin ferric hemoproteins (19,20,35).

The temperature dependence of δ_{DSS}(obs) has been modeled by an equilibrium between the ground state doublet and its thermally populated doublet, which has its magnetic axes rotated by 90° relative to the ground state (19,20,35). This model predicts that increased, less positive Curie slopes for the heme methyl with small δ_{DSS}(obs) as the spacing of the levels increases, with these two methyls exhibiting anti-Curie behavior (negative slope in Curie plot) if the level spacing is large enough. It is noted here that, while 8-CH_3 exhibits anti-Curie behavior (negative Curie slope) for δ_{DSS}(obs), the correction for the δ_{dip}(calc) as a function of temperature leads to a 8-CH_3 δ_{con} with positive Curie slope. Hence, the temperature dependence of δ_{con} suggests a smaller splitting between the two spin doublets than indicated by δ_{DSS}(obs) and confirms the importance of correcting for the dipolar shift (29) before interpreting deviations from Curie behavior in terms of the spacing between the two orbital states.

Lastly, it is observed that each of the meso-Hs exhibit 2–4 ppm low-field δ_{con}, as previously observed for sperm whale metMbCN (29), which is contrary to the difference in the α-/δ-meso versus β-/δ-meso-H δ_{con} as predicted (18) by the prevailing model for hyperfine shifts in low-spin ferric hemins. The failure to account for meso-H δ_{con} patterns in other metMbCN complexes has been noted previously (52). Detailed calculations of the unpaired spin distribution in low-spin ferric hemes have shown that correlation leads to both positive and negative spin density on the heme periphery that cannot be interpreted simply based on MO theory of π-spin density in a single molecular orbital (53) .

Plasticity of *Aplysia* metMbCN

The perfectly linear temperature dependence of hyperfine shifts and magnetic anisotropy over the temperature range through unfolding dictate the absence of partially unfolded intermediates, but do not guarantee a completely temperature-independent molecular structure, as long as the structural change is continuous. The plot of the Euler angles versus temperature in Fig. 6 *A* shows that, whereas direction of tilt, α, and the rhombic axes, $\kappa = \alpha + \gamma$, are invariant, the magnitude of the tilt, β, decreases monotonically with temperature. The difference in β between 5° and 68°C is outside the uncertainties in the values. This is in contrast with observations (29) for sperm whale metMbCN, where the tilt, β, is larger and invariant between 5° and 50°C. Hence, since the major magnetic axes correlates with the Fe-CN vector (10,16), the degree of Fe-CN tilt in sperm whale is temperature-independent, but this Fe-CN tilt is reduced with increasing temperature for *Aplysia* metMbCN. Such an effect indicates that the tilted Fe-CN lies in a steeper potential well in sperm whale than in *Aplysia* metMbCN, or that the distal cavity structure is somewhat more plastic in the latter than the former complex.

These conclusions are in accord with several other experimental data. Thus, protohemin reorients about the α-γ-meso axis much more rapidly (5), and the lability of the axial His(F8) $N_\delta H$ is greater (6) in *Aplysia* than sperm whale metMbCN (54), both of which have been interpreted as representing a dynamically less stable heme cavity structure in the former than the latter myoglobin.

SUPPLEMENTARY MATERIAL

An online supplement to this article can be found by visiting BJ Online at http://www.biophysj.org.

The research was supported by grants from the National Institutes of Health (No. HL 16087 to G.N.L.) and the Ministero Università e Ricerca Scientifica of Italy (No. FIRB 2003, Structural Dynamics of Metalloproteins, to M.B.).

REFERENCES

1. Antonini, E., and M. Brunori. 1971. Hemoglobin and Myoglobin and Their Reactions with Ligands. Elsevier, North-Holland Publishing, Amsterdam, The Netherlands. 40–54.
2. Dickerson, R. E., and I. Geis. 1983. Hemoglobin: Structure, Function, Evolution and Pathology. Benjamin-Cummings, Menlo Park, CA.
3. Griko, Y. V., P. L. Privalov, S. Y. Venyaminos, and V. P. Kutyshenko. 1988. Thermodynamic study of apomyoglobin structure. *J. Mol. Biol.* 202:127–138.
4. Cutruzzolà, F., C. Travaglini-Allocatelli, A. Brancaccio, and M. Brunori. 1996. *Aplysia limacina* myoglobin cDNA cloning—an alternative mechanism of oxygen stabilization as studied by active-site mutagenesis. *Biochem. J.* 314:83–90.
5. Bellelli, A., R. Foon, F. Ascoli, and M. Brunori. 1987. Heme disorder in two myoglobins: comparison of reorientation rates. *Biochem. J.* 246: 787–789.
6. Peyton, D. H., G. N. La Mar, U. Pande, F. Ascoli, K. M. Smith, R. K. Pandey, D. W. Parish, M. Bolognesi, and M. Brunori. 1989. Proton nuclear magnetic resonance study of the molecular and electronic structure of the heme cavity in *Aplysia* cyanomet-myoglobin. *Biochemistry.* 28:4880–4887.
7. Brunori, M., M. Giacometti, E. Antonini, and J. Wyman. 1972. Denaturation of *Aplysia* myoglobin. Equilibrium study. *J. Mol. Biol.* 63:139–152.
8. Staniforth, R. A., M. G. Bigotti, F. Cutruzzolà, C. Travaglini-Allocatelli, and M. Brunori. 1998. Unfolding of apomyoglobin from *Aplysia limacina*: the effect of salt and pH on the cooperativity of folding. *J. Mol. Biol.* 275:133–148.
9. Staniforth, R. A., S. Giannini, M. G. Bigotti, F. Cutruzzolà, C. Travaglini-Allocatelli, and M. Brunori. 2000. A new folding intermediate of apomyoglobin from *Aplysia limacina*: a stepwise formation of a molten globule. *J. Mol. Biol.* 297:1231–1244.
10. La Mar, G. N., J. D. Satterlee, and J. S. de Ropp. 2000. NMR of hemoproteins. *In* The Porphyrins Handbook. K.M. Kadish, K.M. Smith, and R. Guilard, editors. Academic Press, San Diego, CA. 185–298.
11. Nguyen, B. D., Z. Xia, F. Cutruzzolà, C. Travaglini-Allocatelli, A. Brancaccio, M. Brunori, and G. N. La Mar. 2000. Solution ^{1}H NMR study of the active site of *Aplysia limacina* cyanomet myoglobin mutant Val(E7)His/Thr(E10)Arg designed to mimic the sperm whale myoglobin pocket. Influence of distal hydrogen-bonding and N-terminus acetylation on the heme electronic and molecular structure. *J. Biol. Chem.* 275:742–751.
12. Qin, J., and G. N. La Mar. 1992. Complete sequence-specific ^{1}H NMR resonance assignment of hyperfine-shifted residues in the active site of a paramagnetic protein: application to *Aplysia* cyano-metmyoglobin. *J. Biomol. NMR.* 2:597–618.
13. Qin, J., G. N. La Mar, F. Ascoli, M. Bolognesi, and M. Brunori. 1992. Solution ^{1}H NMR determination of hydrogen bonding of the E10(66) Arg side chain to the bound ligand in *Aplysia* cyano-met myoglobin. *J. Mol. Biol.* 224:891–897.
14. Qin, J., U. Pande, G. N. La Mar, F. Ascoli, P. Ascenzi, F. Cutruzzolà, C. Travaglini Allocatelli, and M. Brunori. 1993. ^{1}H NMR study of the dynamics of the pH modulation of axial coordination in *Aplysia limacina* (E7 Val) and sperm whale double mutant His[E7] →Val, Thr[E10]→Arg metmyoglobin: role of distal hydrogen bonding in ligation. *J. Biol. Chem.* 278:4012–4021.
15. Bertini, I., and C. Luchinat. 1996. NMR of paramagnetic substances. *Coord. Chem. Rev.* 150:1–296.
16. Emerson, S. D., and G. N. La Mar. 1990. NMR determination of the orientation of the magnetic susceptibility tensor in cyano met-myoglobin: a new probe of steric tilt of bound ligand. *Biochemistry.* 29: 1556–1566.
17. Horrocks, W. D., Jr., and E. S. Greenberg. 1973. Evaluation of dipolar nuclear magnetic resonance shifts in low-spin hemin systems: ferricytochrome c and metmyoglobin cyanide. *Biochim. Biophys. Acta.* 322: 38–44.
18. Shokhirev, N. V., and F. A. Walker. 1998. The effect of axial ligand plane orientation on the contact and pseudocontact shifts of low-spin ferriheme proteins. *J. Biol. Inorg. Chem.* 3:581–594.
19. Turner, D. L. 2000. Obtaining ligand geometries from paramagnetic shifts in low-spin heme proteins. *J. Biol. Inorg. Chem.* 5:328–332.
20. Turner, D. L., L. Brennan, S. G. Chamberlin, R. O. Louro, and A. V. Xavier. 1998. Determination of solution structures of paramagnetic proteins by NMR. *Eur. Biophys. J.* 27:367–375.
21. Pande, U., G. N. La Mar, J. T. J. Lecomte, F. Ascoli, M. Brunori, K. M. Smith, R. K. Pandey, D. W. Parish, and V. Thanabal. 1986. NMR study of the molecular and electronic structure of the heme cavity of *Aplysia* metmyoglobin. Resonance assignments based on isotope labeling and ^{1}H nuclear Overhauser effect measurements. *Biochemistry.* 25:5638–5646.
22. Jeener, J., B. H. Meier, P. Bachmann, and R. R. Ernst. 1979. Investigation of exchange processes by two-dimensional NMR spectroscopy. *J. Chem. Phys.* 71:4546–4553.
23. Fersht, A. 1999. Structure and Mechanism in Protein Science: A Guide to Enzyme Catalysis and Protein Folding. W. H. Freeman & Company, New York.
24. Myers, J. K., C. N. Pace, and J. M. Scholtz. 1995. Denaturant m values and heat capacity changes: relation to changes in accessible surface areas of protein unfolding. *Protein Sci.* 4:2138–2148.
25. Privalov, P. L., N. N. Kechinashvili, and B. A. Atanossov. 1971. Thermodynamic analysis of thermal transitions in globular proteins. I. Calorimetric study of ribotrypsinogen, ribonuclease and myoglobin. *Biopolymers.* 10:1865–1890.
26. Williams, G., N. J. Clayden, G. R. Moore, and R. J. P. Williams. 1985. Comparison of the solution and crystal structures of mitochondrial cytochrome *c*. Analysis of paramagnetic shifts in the nuclear magnetic resonance spectrum of ferricytochrome *c*. *J. Mol. Biol.* 183:447–460.
27. Press, W. H., B. P. Flannery, S. A. Teukolsky, and W. T. Vetterlin. 1986. Numerical Recipes. Cambridge University Press, Cambridge, UK. 1–795.
28. Shrager, R. I. 1970. Nonlinear regression with linear constraints: an extension of the magnified diagonal method. *J. ACM.* 17:446–452.
29. Nguyen, B. D., Z. Xia, D. C. Yeh, K. Vyas, H. Deaguero, and G. La Mar. 1999. Solution NMR determination of the anisotropy and orientation of the paramagnetic susceptibility tensor as a function of temperature for metmyoglobin cyanide; implications for the population of excited electronic states. *J. Am. Chem. Soc.* 121:208–217.
30. Qin, J., G. N. La Mar, F. Ascoli, and M. Brunori. 1993. Solution NMR determination of active site structure for a paramagnetic protein: cyanomet *Aplysia* Mb. *J. Mol. Biol.* 231:1009–1023.
31. Neal, S., A. M. Nip, H. Zhang, and D. S. Wishart. 2003. Rapid and accurate calculation of protein ^{1}H, ^{13}C and ^{15}N chemical shifts. *J. Biomol. NMR.* 26:215–240.
32. Wishart, D. S., B. D. Sykes, and F. M. Richard. 1991. Relationship between nuclear magnetic resonance chemical shift and protein secondary structure. *J. Mol. Biol.* 222:311–333.
33. Cross, K. J., and P. E. Wright. 1985. Calibration of ring-current models for the heme ring. *J. Magn. Reson.* 64:220–231.
34. Conti, C., C. Moser, M. Rizzi, A. Mattevi, C. Lionetti, A. Coda, P. Ascenzi, M. Brunori, and M. Bolognesi. 1993. X-ray crystal structure of ferric *Aplysia limacina* myoglobin in different ligand states. *J. Mol. Biol.* 233:498–508.
35. Shokhirev, N. V., and F. A. Walker. 1995. Analysis of the temperature dependence of the ^{1}H contact shifts in low-spin Fe^{III} model hemes and

heme proteins: explanation of ''Curie'' and ''anti-Curie'' behavior within the same molecule. *J. Phys. Chem.* 99:17795–17804.

36. La Mar, G. N., J. B. Hauksson, L. B. Dugad, P. A. Liddell, N. Venkataramana, and K. M. Smith. 1991. Proton NMR study of the heme rotational mobility in myoglobin: the role of propionate salt-bridges in anchoring the heme. *J. Am. Chem. Soc.* 113:1544–1550.
37. Walker, F. A. 2000. Proton NMR and EPR spectroscopy of paramagnetic metalloporphyrin. *In* The Porphyrin Handbook. K.M. Kadish, K.M. Smith, and R. Guilard, editors. Academic Press, Boston, MA. 1–183.
38. Bolognesi, M., A. Coda, F. Frigero, G. Gatti, P. Ascenzi, and M. Brunori. 1989. *Aplysia limacina* myoglobin—crystallographic analysis at 1.6 Å resolution. *J. Mol. Biol.* 205:529–544.
39. Horrocks, J. W. D., and E. S. Greenberg. 1974. Isotropic nuclear magnetic resonance shifts in low-spin iron^{III} porphyrin and hemin systems. Theoretical interpretation of temperature dependencies. *Mol. Phys.* 27:993–999.
40. Musto, R., M. G. Bigotti, C. Travaglini-Allocatelli, M. Brunori, and F. Cutruzzolà. 2004. Folding of *Aplysia limacina* apomyoglobin involves an intermediate in common with other evolutionarily distant globins. *Biochemistry.* 43:230–236.
41. Shokhirev, N. V., and F. A. Walker. 1998. Co- and counter-rotation of magnetic axes and axial ligands in low-spin ferriheme systems. *J. Am. Chem. Soc.* 120:981–990.
42. Rajarathnam, K., J. Qin, G. N. La Mar, M. L. Chiu, and S. G. Sligar. 1993. Solution structure determination of the heme cavity in the E7 His → Val cyano-met myoglobin point mutant based on the ^{1}H NMR detected dipolar field of the iron: evidence for contraction of the heme pocket. *Biochemistry.* 32:5670–5680.
43. Kuriyan, J., S. Wilz, M. Karplus, and G. A. Petsko. 1986. X-ray structure and refinement of carbon-monoxy (Fe^{II})-myoglobin at 1.5 Å resolution. *J. Mol. Biol.* 192:133–154.
44. Du, W., Z. Xia, S. Dewilde, L. Moens, and G. N. La Mar. 2003. ^{1}H NMR study of the molecular structure and magnetic properties of the active site for the cyanomet complex of O_2-avid hemoglobin from the trematode *Paraphistomum epiclitum*. *Eur. J. Biochem.* 270:2707–2720.
45. Lee, K.-B., G. N. La Mar, K. E. Mansfield, K. M. Smith, T. C. Pochapsky, and S. G. Sligar. 1993. Interpretation of hyperfine shift patterns in ferricytochromes b5 in terms of angular position of the heme: a sensitive probe for peripheral heme protein interactions. *Biochim. Biophys. Acta.* A1202:189–199.
46. Wu, Y., E. Y. T. Chien, S. G. Sligar, and G. N. La Mar. 1998. Influence of proximal side mutations on the molecular and electronic structure of cyanomet myoglobin: a ^{1}H NMR study. *Biochemistry.* 37:6979–6990.
47. Xia, Z., B. D. Nguyen, and G. N. La Mar. 2000. The use of chemical shift temperature gradients to establish the paramagnetic susceptibility tensor orientation: implication for structure determination/refinement in paramagnetic metalloproteins. *J. Biomol. NMR.* 17:167–174.
48. Xia, Z., W. Zhang, B. D. Nguyen, A. P. Kloek, D. E. Goldberg, and G. N. La Mar. 1999. ^{1}H NMR investigation of the distal hydrogen bonding network and ligand tilt in the cyanomet complex of oxygen-avid *Ascaris* hemoglobin. *J. Biol. Chem.* 274:31819–31826.
49. Hargrove, M. S., J. K. Barry, E. A. Bricker, M. B. Berry, G. N. Phillips, Jr., J. S. Olson, R. Peter-Arredondo, J. M. Dean, R. V. Klucas, and G. Sarath. 1997. Characterization of recombinant soybean leghemoglobin a and apolar distal histadine mutants. *J. Mol. Biol.* 266:1032–1042.
50. La Mar, G. N., S. D. Emerson, J. T. J. Lecomte, U. Pande, K. M. Smith, G. W. Craig, and L. A. Kehres. 1986. The influence of propionate side chains on the equilibrium heme orientation in sperm whale myoglobin. Heme resonance assignments and structure determination by nuclear Overhauser effect measurements. *J. Am. Chem. Soc.* 108:5568–5573.
51. Mayer, A., S. Ogawa, R. G. Shulman, T. Yamane, J. A. S. Cavaleiro, A. M. D. A. Rocha Gonsalves, G. W. Kenner, and K. M. Smith. 1974. Assignment of the paramagnetically shifted heme methyl nuclear magnetic resonance peaks of cyanomet-myoglobin by selective deuteration. *J. Mol. Biol.* 86:749–756.
52. Hu, B., J. B. Hauksson, A.-T. Tran, U. Kolczak, R. K. Pandey, K. Smith, and G. N. La Mar. 2001. ^{1}H and ^{13}C NMR investigation of the influence of non-ligated residue contacts on the heme electronic structure in cyano-metmyoglobin complexes reconstituted with centro- and pseudo-centro-symmetric hemins. *J. Am. Chem. Soc.* 123:10063–10070.
53. Johansson, M. P., D. Sundholm, G. Gerfen, and M. Wilkström. 2002. The spin distribution in low-spin iron porphyrins. *J. Am. Chem. Soc.* 124:11771–11780.
54. La Mar, G. N., J. D. Cutnell, and S. B. Kong. 1981. Proton magnetic resonance characterization of the dynamic stability of the heme pocket in myoglobin by the exchange behavior of the labile proton of the proximal histidyl imidazole. *Biophys. J.* 34:217–226.